Monte Carlo Model for Determination of the Role of Heat Generation in Laser-Irradiated Tissue

A. J. Welch

C. M. Gardner

Biomedical Engineering Program,
The University of Texas at Austin,
Austin, TX 78712

A Monte Carlo model is described for modeling photo propagation in a scattering medium. The fraction of locally absorbed photons is proportional to the local rate of heat generation in laser-irradiated tissue and the associated distribution of light (fluence rate) is obtained by dividing the rate of heat generation by the local absorption coefficient. Examples of computed distributions of the rate of heat generation are presented for situations where light scattering in tissue is important. The method is applied to analyze treatment of Port Wine Stain and the selection of laser wavelengths for cyclophotocoagulation.

Introduction

The thermal response of tissue to laser irradiation is driven by the rate of volumetric energy absorption [W/m^3] resulting from the absorption of the laser light. The spatial distribution of the light absorption is a function of the diameter and penetration depth of the laser beam. The distribution of light is governed by the wavelength-dependent absorption and scattering properties of the medium. The absorbed energy can be modeled as internal energy generation. The rate of heat generation of a selected target volume within tissue is directly proportional to the local light fluence rate ϕ[W/m^2] and the local absorption coefficient μ_a[1/m]. The fluence rate includes the collimated light from the laser beam and diffuse light scattered from the beam. When light scattering is significant, Beer's law (exponential attenuation) cannot be used to describe the attenuation of light with depth. For tissue, scattering is significant over the visible and near-infrared wavelengths.

In this paper, we describe the typical light-tissue interactions and governing equations of light propagation in tissue. Next we describe a Monte Carlo model for estimating the rate of heat generation $S(r)$[W/m^3] and fluence rate $\phi(r)$. Two examples are presented to illustrate the importance of computing reasonable estimates of the local rate of heat generation in the selection of laser parameters.

Model for Laser-Tissue Interaction. The overall interaction of light with tissue is shown in Fig. 1. As light strikes tissue, a portion of the light is reflected based upon the angle of incidence (Snell's law) and index of refraction of the air and of the tissue (Fresnel equation). For normal incident light this is about 2.5 percent. Light that enters tissue undergoes scattering and absorption. It is the absorbed photons that generate heat within the tissue. The propagation of light in tissue that reaches a boundary is governed by Fresnel's equation. For example, light within tissue striking an air ($n_1 = 1$) – tissue ($n_2 = 1.4$) interface will be totally internally reflected if the angle of the light is greater than the critical angle $\theta_c = \arcsin(n_1/n_2)$. In this example, the critical angle is about 46 deg with respect to the normal to the surface. If scattering dominates absorption, light is scattered from the laser beam, creating diffuse light in the tissue. This diffuse light will be absorbed, backscattered to the anterior surface, or transmitted through the tissue. Once again, diffuse light that is absorbed generates heat. When Caucasian skin is irradiated with 600 nm light, approximately 40 percent of the light is remitted (backscattered) from the skin since scattering dominates absorption at this wavelength (Anderson and Parrish, 1981).

For any tissue, there is considerable variation in light penetration depth (magnitude of e^{-1} relative to irradiance) with wavelength owing to the wavelength dependent optical properties. This is illustrated in Fig. 2 for soft tissue such as dermis, aorta, muscle, etc. The penetration values (given at the arrowheads) are approximate for a class of tissue. Estimated values of absorption for some of the primary chromophores in tissue (water, oxygenated hemoglobin (HbO_2), protein and amino acids, and melanin) are presented in Fig. 3. As noted in the figure, absorption generally dominates scattering for wavelengths below 350 nm and above 1500 nm owing to absorption of proteins and amino acids in the UV spectrum and water in the IR spectrum. In contrast, the wavelengths between 600 nm and 1100 nm provide a window for light penetration in tissue. Absorption is low and the resulting radiance of light is the result of multiple scattering.

The important light propagation term relative to heat generation is the fluence rate $\phi(r)$ [W/m^2]. The fluence rate represents the amount of collimated and diffuse light passing through a small volume at point r in any direction. The fluence rate at a point $r[r = x, y, z]$ is

$$\phi(r) = \int_{4\pi} L(r, s')d\Omega' \tag{1}$$

where s' is the unit direction of the radiance, L[$W/m^2 - sr$]. The radiance can be computed from the transport equation (see Eq. (4)), which describes the propagation of light power in a turbid medium (Ishimaru, 1978).

The rate of heat generation in laser-irradiated tissue is due to the absorption of the laser light and conversion of light energy to heat. At a point r the rate of heat generation is equal to the local fluence rate times the local absorption coefficient (Welch and van Gemert, 1995):

$$S(r) = \phi(r)\mu_a(r) \tag{2}$$

The absorption coefficient μ_a[1/m] is defined such that $1/\mu_a$ is the distance over which light is attenuated by $1/e$ due to absorption. Thus to estimate the rate of heat generation at position r in laser irradiated tissue, it is necessary to know the

Contributed by the Bioengineering Division for publication in the JOURNAL OF BIOMECHANICAL ENGINEERING. Manuscript received by the Bioengineering Division March 13, 1996; revised manuscript received November 14, 1996. Associate Technical Editor: J. J. McGrath.

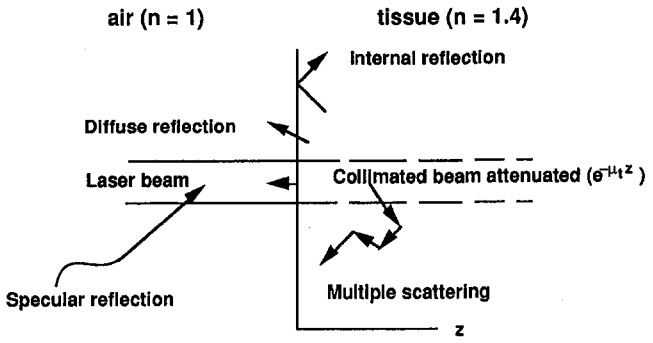

Fig. 1 Optical interaction of collimated laser beam with tissue. Specular reflection for air–tissue interface is approximately 2.5 percent when laser beam is normal to tissue that has an index of refraction of 1.4. Multiple scattering creates diffuse light in the tissue. The portion of diffuse light that exits the tissue produces diffuse reflection. Collimated light is attenuated exponentially ($e^{-\mu_t z}$) where $\mu_t = \mu_a + \mu_s$.

absorption coefficient $\mu_a(r)$ and determine the fluence rate $\phi(r)$ which depends upon the geometry and optical properties of the tissue.

If absorption dominates scattering ($\mu_a \gg \mu_s$, where μ_s is the scattering coefficient), then the fluence rate can be approximated by the exponential attenuation of the collimated laser beam. That is, for a uniform irradiance onto a homogeneous semi-infinite plane, light propagation is governed by Beer's law, which describes the attenuation of the collimated laser beam $\phi_c(z)$ as

$$\phi_c(z) = E_0 e^{-\mu_a z} \tag{3}$$

where E_0 is the laser irradiance [W/m^2] neglecting specular reflection at the surface. This equation is suitable for wavelengths below 300 nm and above 1500 nm. In fact, it is a good estimate of the total fluence under the laser beam as long as $\mu_s < \mu_a$ (Welch and Gardner, in press).

However, for wavelengths between 450 nm and 1100 nm light is usually scattered in soft tissue. Especially from 600 nm to 1000 nm there is a broad minimum in the absorption spectrum of soft tissue. At these wavelengths light can be detected several centimeters into tissue. When scattering dominates absorption, the fluence rate of scattered light may be much larger than the collimated light throughout the tissue. The radiance, L, of scattered light is estimated using an approximation or a simulation of the transport equation. This governing equation for light propagation in a turbid medium is

$$(s \cdot \nabla)L(r, s) = -\mu_t L(r, s) + \mu_s \int_{4\pi} p(s, s')L(r, s')d\Omega' \ [\mathrm{W/m^3 \cdot sr}] \tag{4}$$

where μ_t is the attenuation coefficient ($\mu_t = \mu_a + \mu_s$). The radiance at r in the s direction is decreased by absorption and scattering but increased due to light at position r that is scattered from the s' directions to the s direction. The phase function $p(s, s')$ [$1/sr$] is a single scattering probability density function for scattering angle. By assuming tissue is homogeneous and isotropic, the scattering from s' to s can be represented by the angle between s and s'. That is,

$$p(s, s') = p(s \cdot s')p(\phi) = p(\cos\theta)p(\phi) \tag{5}$$

where θ is the angle between s and s' and ϕ is the angle about s. $p(\cos\theta)$ describes the forward scattering nature of light in tissue and $p(\phi)$ is uniformly distributed over the 2π rad at s. Typically $p(\cos\theta)$ is described by the Henyey–Greenstein relation, which is a function of the expected (average) cosine of the scattering angle, g.

$$g = \tfrac{1}{2}\int_{-1}^{+1} p(\cos\theta)\cos\theta d\cos\theta \tag{6}$$

Descriptions of solutions for this equation may be found in Ishimaru (1978) and Welch and van Gemert (1995).

Monte Carlo Model. The rate of heat generation can be estimated using a Monte Carlo simulation of Eq. (4) when the equation has been integrated over 4π sr. The unknown in a direct solution of Eq. (4) is the radiance L[W/m$^2 \cdot sr$]. Integrating L over 4π sr yields the fluence rate ϕ[W/m^2] (Welch and van Gemert, 1995). Monte Carlo models provide better accuracy near surfaces and the collimated laser beam than the faster diffusion approximation of Eq. (4). The model contains two parts. The first describes the distribution of photons for a ray of light normal to the tissue surface. This ray has zero radius and is represented as a packet of N photons that are released one at a time. The resulting scaled pattern of absorbed photons in a cylindrical geometry r, z is the ray response $G(r, z)$ of the tissue. The rate of heat generation for a finite laser beam is computed by convolving the ray response and the radial irradiance profile $E_0(r)$ of the laser beam.

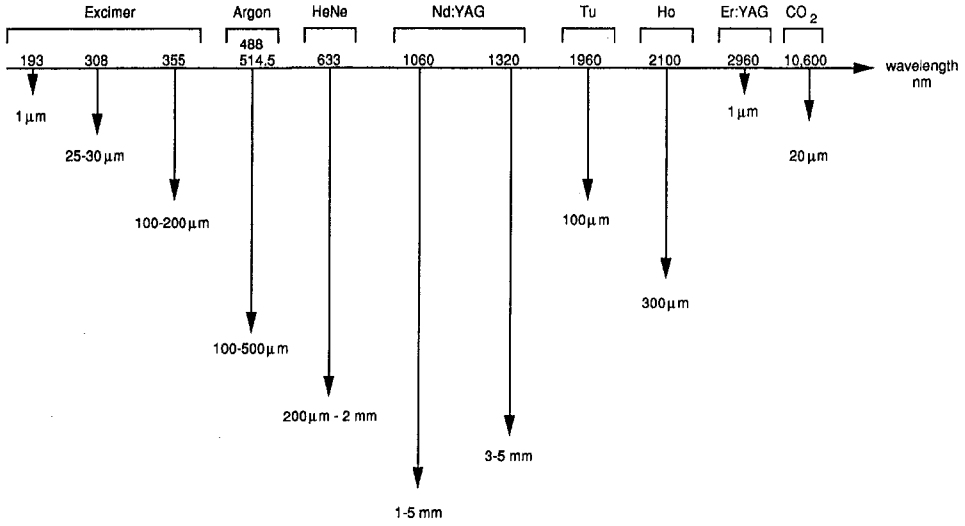

Fig. 2 Optical penetration depth of light in soft tissue (approximately $1/\mu_{eff}$ for dominant scattering where $\mu_{eff} = \sqrt{3\mu_a[\mu_a + \mu_s(1 - g)]}$)

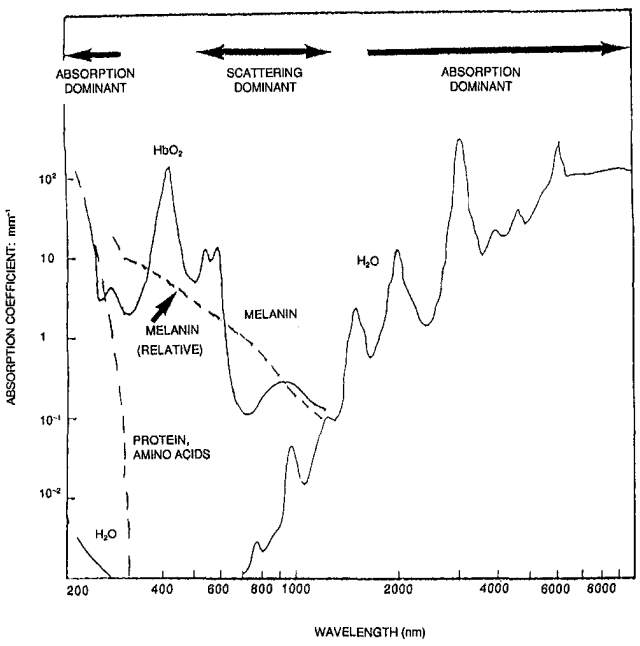

Fig. 3 Absorption coefficient for (*a*) proteins and amino acids, (*b*) oxygenated hemoglobin, (*c*) melanin, and (*d*) water in units of mm^{-1}. Modified from Boulnois (1986).

$$S(r, z) = G(r, z) * E(r) = \int_0^\infty S(r') \times \left[\int_0^{2\pi} G(\sqrt{r^2 + r'^2 - 2rr' \cos \alpha'}, z) d\alpha' \right] r' dr' \quad (7)$$

The fluence rate is obtained by dividing $S(r, z)$ by $\mu_a(r, z)$. Thus the Monte Carlo model provides a two-dimensional (r, z) estimate of the fluence rate and rate of heat generation for a set of optical properties and an irradiance profile. Once the heat source is determined, it can be placed in a numerical model of the heat conduction equation to compute tissue temperature response to laser irradiation. The influence of wavelength is determined by computing the "ray" response for appropriate sets of wavelength dependent optical properties. A sketch of the Monte Carlo Model is given in the appendix. Further detail is given by Welch and van Gemert (1995) and Keijzer et al. (1989).

Example of Monte Carlo Simulation. An example of Monte Carlo modeling is presented in Fig. 4. The code used in this simulation has been validated against code published by Wang and Jacques (1992), and provides values of reflectance and transmittance within 0.5 percent of values obtained with analytic solutions of Eq. (4) for semi-infinite slabs with matched or mismatched boundary conditions (Welch and van Gemert, 1995). In this example a semi-infinite slab of homogeneous tissue is irradiated by a normally incident gaussian beam:

$$E(r) = e^{-2r^2/W_0^2} \quad (8)$$

where W_0 is the $1/e^2$ radius. We assume $W_0 = 1$ mm and a highly scattering medium ($\mu_a = 1$ cm^{-1}; $\mu_s = 999$ cm^{-1}), and light is scattered anisotropically such that the average cosine of the scattering angle is $g = 0.875$. The simulation geometry approximates a semi-infinite plane with an air–tissue interface ($n_1 = 1.4$; $n_2 = 1.0$). Computed two-dimensional constant fluence rate [W/cm^2] contour plots for $E_0 = 1$ W/cm^2 are presented in Fig. 4(a, b). Figure 4(b) is an expanded view for $0 < r < 1$ and $0 < z < 1$. For z greater than 1 mm there is the expected decay in exponential fluence rate far from the surface. The peak fluence rate just below the tissue surface ($z = 0+$) is 4.9 W/cm^2, which is due to the multiple scattering that takes place. Energy is conserved over the entire volume, but near the surface the rate of heat generation [W/cm^3] is much larger than expected. That is, $\mu_a\phi\ (z = 0+) > \mu_a E_0$ at $r = 0$. In this example the rate of heat generation is 4.9 times larger than would be estimated by a simple Beer's law approximation. This is consistent with the result obtained from diffusion theory (Flock et al., 1989).

Medical Applications. Many photothermal applications occur at wavelengths (450–1100 nm) at which scattering dominates absorption. For example, the Nd:YAG laser at 1064 nm,

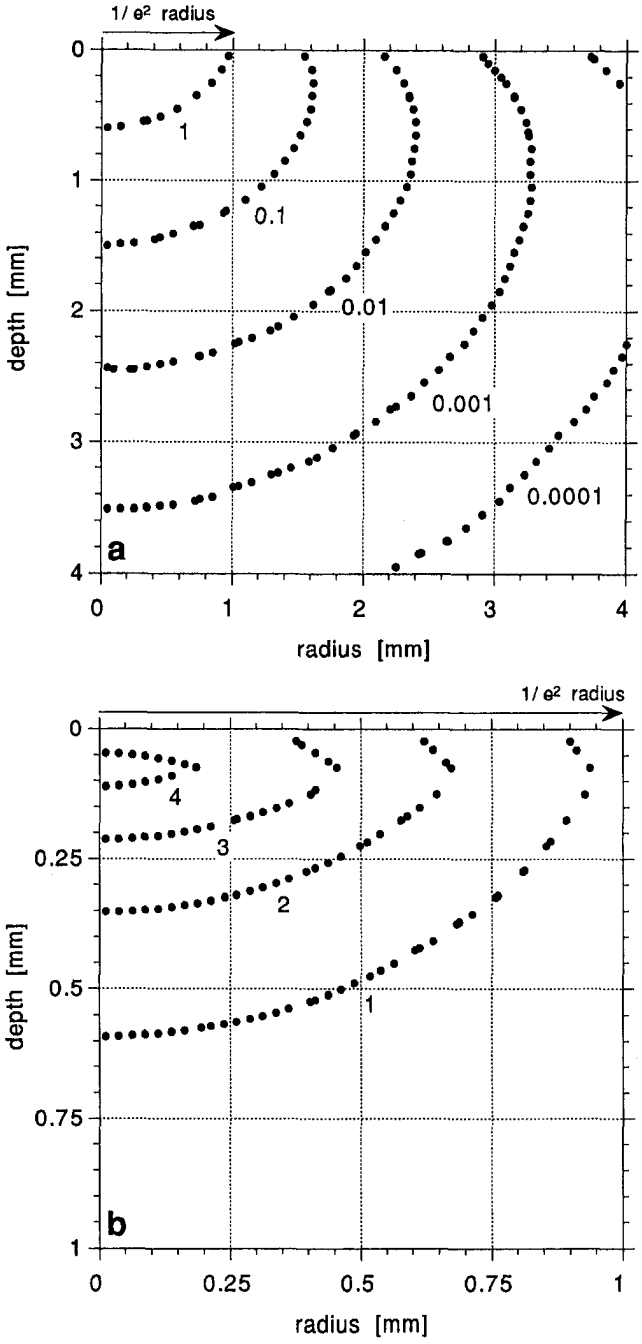

Fig. 4 Monte Carlo simulation for a 2 mm $1/e^2$ diameter normally incident gaussian beam on a semi-infinite, homogeneous tissue slab. Tissue optical properties are $\mu_a = 1$ cm^{-1}, $\mu_s = 999$ cm^{-1}, $g = 0.875$, $n_{tissue} = 1.4$, $n_{air} = 1.0$. (*a*) Contour plot of fluence rate normalized to peak source irradiance. (*b*) Expanded contour plot of fluence rate normalized to peak source irradiance for depths between 0 and 1 mm.

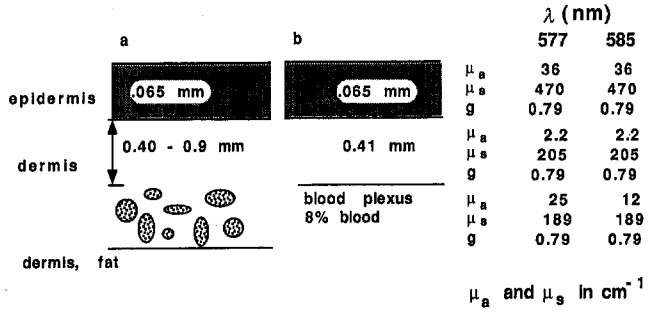

Fig. 5 Geometry for modeling Port Wine Stains: (*a*) enlarged blood vessels are located in the blood plexus layer of dermis; (*b*) to illustrate the effect of wavelength upon PWS treatment, the blood plexus is modeled as a homogeneous layer. Its optical properties are an average of dermis and blood optical properties based upon volume of each component.

which is available in most large hospitals, is typically used for photocoagulation of soft tissue. A general description of many medical applications of lasers can be found from Welch and van Gemert (1995). Also, a series of review articles describing medical applications of lasers has been published in *Lasers in Surgery and Medicine* from Vol. 15, No. 2 in 1994 through Vol. 17, No. 3 in 1995.

The application of the Monte Carlo techniques to estimate the rate of heat generation during laser heating is illustrated with the following two examples:

1 Treatment of Port Wine Stain
2 Cyclophotocoagulation

1 Treatment of Port Wine Stain. Port Wine Stain is a birth defect that produces a reddish brown mark owing to enlarged vessels in the skin. PWS most often occurs on the face and neck. The color of PWS becomes bluish-red with age, and the surface of the skin becomes rough. The goal of treatment is coagulation of the enlarged vessels with minimal damage to surrounding tissue. The target for the laser irradiation and region where we want the maximum rate of heat generation is the blood inside the vessels. A layered representation of the skin is presented is presented in Fig. 5. For light to reach the blood vessels, it is impossible to avoid absorption in the epidermis, which contains brown melanin pigment. Given that epidermal and dermal scattering and absorption decreases with wavelength and the goal is to maximize heat generation in the blood vessels, the 577 nm peak of the blood absorption curves appears to be the best candidate wavelengths for treatment of PWS (see Fig. 3). Yet clinical trials have shown that 585 nm is more effective (Tan et al., 1990). At 585 nm, the absorption coefficient is one half the value at 577 nm (see Fig. 3).

The relative rate of heat generation has been calculated for the two wavelengths (577 nm and 585 nm) for a gaussian beam with W_0 = 1.0 mm using a Monte Carlo model. We assume there is little change in the optical properties of epidermis or dermis from 577 to 585 nm. All wavelength-dependent changes in optical properties occur in the absorption coefficient of the blood. The blood vessels are represented as a homogeneous blood plexus layer (dermis with blood content of 8 percent). The geometry for the model is presented in Fig. 5 along with the optical properties for the two wavelengths taken from van Gemert and Welch (1991). Computed fluence rate and rate of heat generation along the beam centerline (r = 0, z) are presented in Fig. 6. The fluence is normalized relative to the peak irradiance. Nevertheless, normalized fluence rates to a depth of 0.2 mm exceed 1.0 because of scattering in the dermis.

From Fig. 6, the rate of heat generation at the anterior surface of the blood plexus layer is higher at 577 nm, but the 577 nm curve falls below the 585 nm curve at a plexus thickness of about 250 μm. Clinical results suggest that anterior vessels shield posterior vessels, limiting the effective depth of treatment using 577 nm (Tan et al., 1990). The rate of heat generation in the blood plexus layer does not represent the rate of heat generation in an individual vessel since the absorption coefficient for the layer represents 8 percent blood and 92 percent in dermis.

Present concerns in the laser treatment of Port Wine Stains include determining the optimum treatment wavelength. The Monte Carlo simulation results presented in Fig. 6(a) demonstrates that the average fluence rate of light near a vessel in the blood plexus layer will be greater for 585 nm light than 577 nm light. However, the absorption of 585 nm light by blood is less than absorption of 577 nm light by a factor of approximately 2. The product of these two factors is shown in Fig. 6(b), where 577 nm light produces higher heat generation rates for shallow vessels and the 585 nm light produces higher rates for vessels below a depth of 0.65 mm.

Note that the rate of heat generation in the blood plexus layer was less than the rate at the skin surface. This in reality is not the case, because in the Monte Carlo model the rate of heat generation for 100 percent blood concentration was not computed. The 8 percent blood concentration was uniformly distrib-

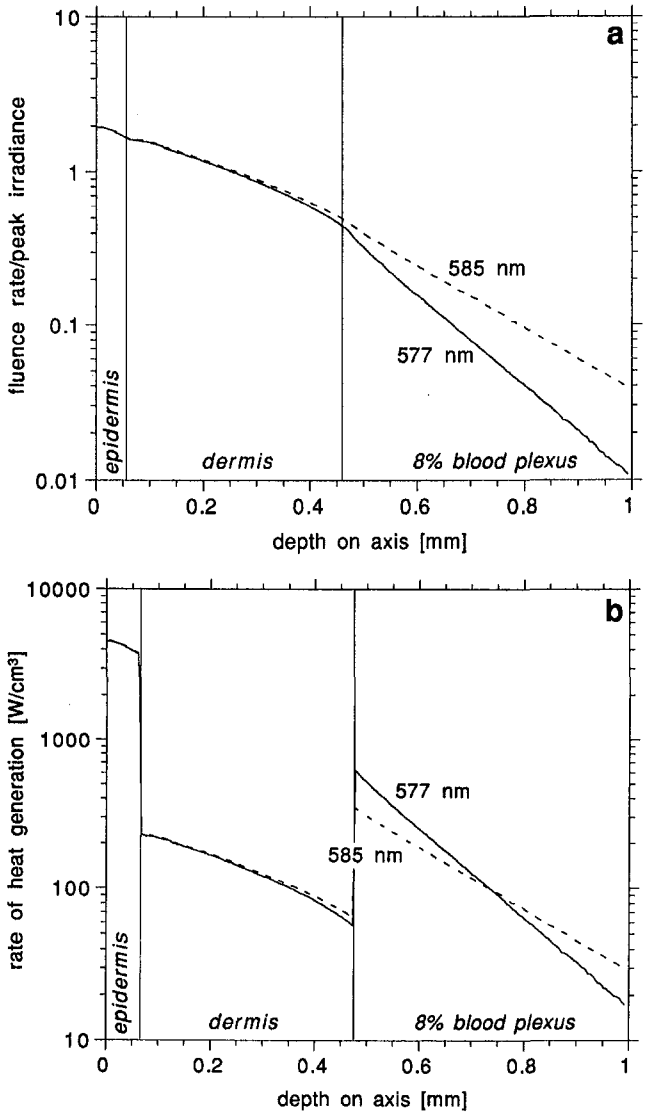

Fig. 6 Monte Carlo simulation for PWS. Layer optical properties are given in Fig. 5. The light source is a 2 mm $1/e^2$ diameter normally incident gaussian beam, with 1 *W* total beam power, and wavelength of 577 nm or 585 nm. (*a*) Fluence rate normalized to peak source irradiance versus tissue depth on axis (r = 0 mm). (*b*) Rate of heat generation versus tissue depth on axis (r = 0 mm).

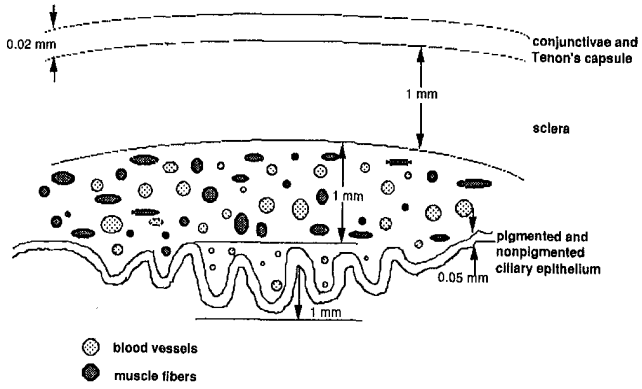

Fig. 7 Cross section of ciliary body

uted in the plexus layer. The actual rate of heat generation at the surface of a blood vessel is

$$S(\text{blood}) = \frac{\mu_a(\text{blood})}{\mu_a(\text{blood plexus})} S(\text{blood plexus}) \quad (9)$$

that is, the rate of heat generation is scaled by the absorption of blood relative to the absorption of the blood plexus layer.

The problem of Port Wine Stain treatment is further complicated by the actual absorption of laser light within vessels, which is a function of the wavelength-dependent optical properties of blood and the direction of light striking the vessels. The $1/e$ optical penetration depth in blood is about 30 μm at 577 nm and 60 μm at 585 nm; typical dimensions for Port Wine Stain vessels are 50–200 μm. Thus the center of large vessels are shielded and anterior vessels shield posterior vessels. An illustration of these effects are given by Lucassen et al. (1996). Needed is a better understanding of the heating conditions that will cause constriction of vessels. Usually we assume heating of the vessel wall is critical for coagulation of a vessel.

Using a blood plexus representation for blood, the 585 nm light maintains a vessel heat source larger than the epidermal heat source, at greater depths than 577 nm light. 585 nm light reduces the effects of shadowing and vessels are more uniformly heated relative to 577 nm radiation.

2 Cyclophotocoagulation. Transcleral cyclophotocoagulation is a photothermal laser treatment of chronic glaucoma. This form of glaucoma is caused by a continual increase of ciliary fluid volume between the lens and iris of the eye. This laser treatment is used as a last resort after other treatments have failed; its goal is to destroy the ciliary body that produces the fluid. The general tissue geometry through which the laser light must travel is shown in Fig. 7. A small beam enters the eye near the outer edge of the iris, passing through the conjuctiva, sclera, and the blood-rich muscle layer of the ciliary body. The target of heat generation is the melanin-pigmented ciliary epithelium.

Since the ciliary epithelium is the primary site of desired heat damage, an ideal laser treatment might employ a wavelength that is highly absorbed by melanin and not absorbed by blood (in the muscle layer), water (below the epithelium), and other tissue components. In addition, scattering must be considered that attenuates the laser light.

Current cyclophotocoagulation treatment employs a Nd:YAG laser with wavelength of 1064 nm. However, because of its availability and cost, the all-lines argon laser with primary lines at 488 nm and 514.5 nm should be considered. A preliminary comparison of the light distributions and rates of heat generation when using Nd:YAG laser light versus laser argon light at 500 nm was made to estimate the merits of each laser. The tissue geometry used for Monte Carlo modeling of cyclophotocoagulation, along with estimated layer by layer optical properties, are presented in Fig. 8. Optical properties were extrapolated from values obtained by Nemati et al. for 1050 nm and 500 (Nemati et al., 1996). The values selected were based on experimental data obtained from *in vitro* samples of conjunctiva, sclera, and ciliary body extracted from rabbit eyes. Figure 9 displays the wavelength dependent fluence rate and heat generation rate.

The rate of heat generation is the product of the fluence rate and the absorption coefficient. For a target site such as melanin in the ciliary pigment epithelium, damage by heat requires either a large fluence rate, or high absorption, or a combination of both. The cyclophotocoagulation model presented in this paper demonstrates that there is an approximately five orders of magnitude of argon light attenuation because of scattering and absorption in the sclera and the ciliary muscle/blood plexus layers. The fluence rate of the Nd:YAG radiation at the pigmented melanin is over 100 times the fluence rate of the argon radiation when the same irradiance is applied to the sclera. The blood content of the ciliary muscle layer highly absorbs the 500 nm radiation, but does not significantly affect the 1064 nm light, as illustrated by the hemoglobin absorption spectra in Fig. 3. The rate of heat generation just below the anterior surface of the pigmented layer differs by a factor greater than 100 for the two wavelengths.

Jacques and McAuliffe (1991) have recently reported that the absorption coefficient of melanin decreases exponentially with wavelength. In fact, absorption by melanin of 500 nm light is at least 2.5 times the absorption at 1064 nm. This difference, which is not sufficient to overcome the attenuation of the argon wavelength by itself, will always favor shorter wavelengths.

Note, the rate of heat generation for the Nd:YAG wavelength is distributed somewhat evenly, whereas heating associated with the argon laser is confined to the sclera and anterior portion of the ciliary muscle. Heat generation is not confined to the targeted pigmented ciliary body.

The results from the Monte Carlo simulation suggest that Nd:YAG radiation is more effective than argon radiation for cyclophotocoagulation. Thus, argon lasers generally available for retinal photocoagulation should not be used for cyclophotocoagulation if the goal is coagulation of the ciliary pigmented layer.

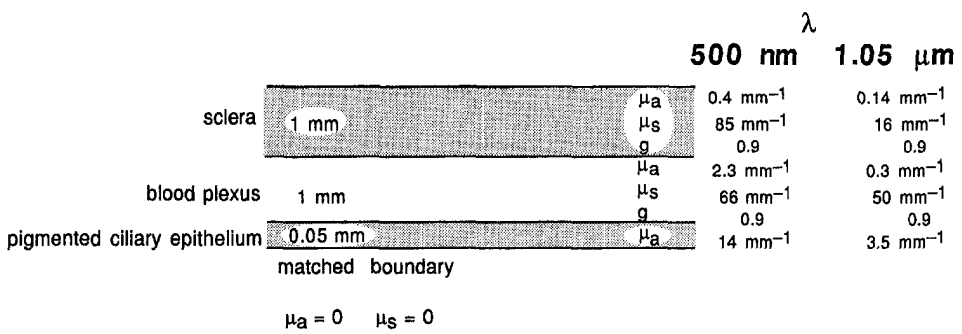

Fig. 8 Geometry for Monte Carlo model for cyclophotocoagulation. Optical properties for argon laser and Nd:YAG laser wavelengths are taken from spectrophotometer measurements at 500 nm and 1050 nm, respectively, of *in vitro* ciliary body obtained from rabbits (Nemati et al., 1996).

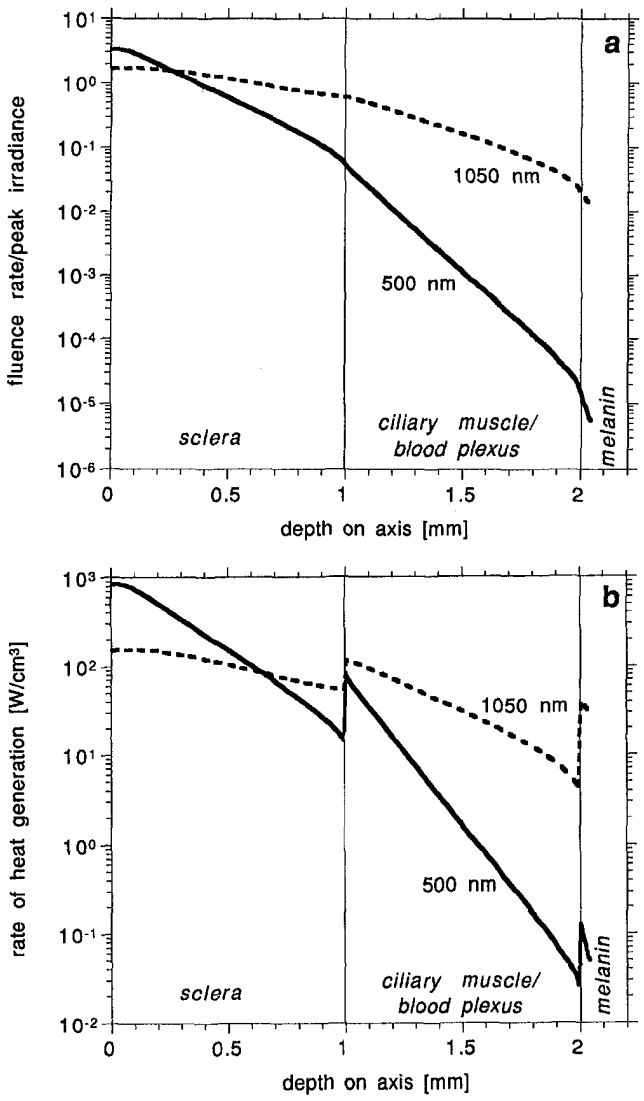

Fig. 9 Monte Carlo cyclophotocoagulation simulation. Layer optical properties are given in Fig. 8. The light source is a 2 mm $1/e^2$ diameter normally incident gaussian beam, with 1 *W* total beam power, and wavelength of 500 nm or 1050 nm. (*a*) Fluence rate normalized to peak source irradiance versus tissue depth on axis (r = 0 mm). (*b*) Rate of heat generation versus tissue depth on axis (r = 0 mm).

Conclusion

Monte Carlo simulation of light propagation provides an accurate assessment of the pattern of photon absorption if optical properties and geometry of the model are reasonable representations of the tissue. This pattern yields the rate of heat generation that is critical for modeling the thermal response of tissue to laser radiation (Welch and van Gemert, 1995).

As illustrated in the examples: (1) single exponential absorption of light with depth does not account for the effects of multiple scattering; and (2) by comparing simulations for various sets of wavelength dependent optical properties, it is possible to compare wavelengths to maximize the rate of heat generation in a target layer of tissue while minimizing heating in surrounding tissue.

References

Anderson, R. R., and Parrish, J. A., 1981, "The Optics of Human Skin," *J. Invest. Dermatol.,* Vol. 77, pp. 13–19.

Boulnois, J.-L., 1986, "Photophysical processes in recent medical laser developments: a review," *Lasers Surg. Med.,* Vol. 1(1), pp. 47–66.

Flock, S. T., Patterson, M. S., Wilson, B. C., and Wyman, D. R., 1989, "Monte Carlo modeling of light propagation in highly scattering tissues—I: Model predictions and comparison with diffusion theory," *IEEE Trans. Biomed. Eng.,* Vol. 36(12), pp. 1162–1167.

Ishimaru, A., 1978, *Wave Propagation and Scattering in Random Media,* Vol. 1, Academic Press, New York.

Jacques, S. L., and McAuliffe, D. J., 1991, "The Melanosome: Threshold Temperature for Explosive Vaporization and Internal Absorption Coefficient During Pulsed Laser Irradiation," *Photochem Photobiol.,* Vol. 53, pp. 769–775.

Keijzer, M., Jacques, S. L., Prahl, S. A., and Welch, A. J., 1989, "Light Distributions in Artery Tissue: Monte Carlo Distributions for Finite Laser Beams," *Lasers Surg. Med.,* Vol. 9, pp. 148–154.

Lucassen, G. W., Verkruysse, W., Keijzer, M., and van Gemert, M. J. C., 1996, "Light Distributions in a Port Wine Stain Model Containing Multiple Cylindrical and Curved Blood Vessels," *Lasers Surg. Med.,* Vol. 18, pp. 345–357.

Nemati, B., Rylander, H. G., III, Welch, A. J., 1996, "Optical Properties of Conjunctiva, Sclera, and Ciliary Body and Their Consequences for Transscleral Cyclophotocoagulation," *Applied Optics,* Vol. 35(19), pp. 3321–3327.

Tan, O. T., Morrison, P., and Kurban, A. K., 1990, "585 nm Treatment for Portwine Stains," *Plast. Reconstr. Surg.,* Vol. 86, pp. 1112–1119.

van Gemert, M. J. C., and Welch, A. J., 1991, "Can Physical Modeling Lead to an Optimal Laser Treatment Strategy for Port Wine Stains?" in: *Laser Applications in Medicine and Biology,* R. W. Waynant, ed., Plenum Press, New York, Vol. 5, pp. 189–276.

Wang, L. H., and Jacques, S. L., 1992, "Monte Carlo modeling of light transport in multi-layered tissues in standard C," University of Texas, M.D. Anderson Cancer Center.

Welch, A. J., and Gardner, C. M., in press, "Optical and Thermal Response of Tissue to Laser Radiation," in: *Lasers in Medicine,* R. W. Waynant, ed., Plenum Press, New York.

Welch, A. J., and van Gemert, M. J. C., eds., 1995, *Optical-Thermal Response of Laser-Irradiated Tissue,* Plenum Press, New York.

APPENDIX

Algorithm for Monte Carlo Model

In its simplest form, each photon is moved a fixed distance Δs until the photon is absorbed or leaves the tissue. A record

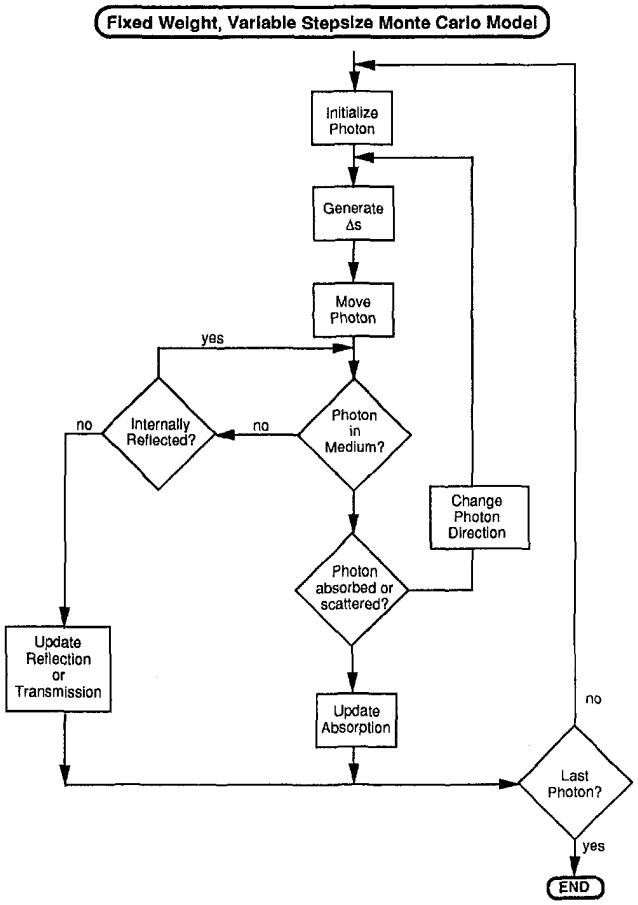

Fig. A-1 Flow graph of variable weight, variable distance Monte Carlo model for photon scattering in turbid medium. Photons are injected normal to tissue.

is kept of the number and location of photons absorbed, number reflected, and for a finite thickness tissue, the number transmitted. The distance Δs must be much smaller than the optical depth, $1/\mu_t$. The key to Monte Carlo simulation is the generation of random numbers between 0 and 1. The numbers (called RAN in this paper) represent an equally likely value of the probability distributions for distance, scattering angles, reflectance, absorption events, and scattering events.

Step 1. Inject photon a distance of Δs normal to the tissue.

Step 2. Use a random number generator with uniform distribution [0, 1] to determine if the photon is absorbed (RAN $\leq \Delta s \mu_a$), scattered, ($\Delta s \mu_a <$ RAN $\leq \Delta s \mu_s + \Delta s \mu_a$) or no interaction ($\Delta s \mu_a + \Delta s \mu_s <$ RAN ≤ 1).

- (a) If absorbed, note location and inject new photon at the surface.
- (b) If no interaction, move photon Δs in the same direction and repeat Step 2.
- (c) If scattered, use random numbers to determine the scattering angle, then move Δs in the new direction and repeat Step 2.

A complete algorithm includes reflections at boundaries when there is a mismatch in the index of reflection. The probability for reflection is obtained from the Fresnel reflection equation and Snell's law (Welch and van Gemert, 1995), and once again a random number is used to decide if a photon is internally reflected or transmitted through a boundary.

The accuracy and speed of the algorithm are improved by incorporating variable weight photons and variable movement intervals as illustrated in the flow chart of Fig. A-1. The theoretical range of distance for the movement intervals is $[0, \infty]$ with an expected (probability weighted average) distance of $1/\mu_t$. Movement Δs is given as $\Delta s = -\ln [\text{RAN}]/\mu_t$. After each displacement the photon weight is reduced because of absorption by the fraction $(\mu_a/(\mu_a + \mu_s))$ and the remaining portion of the photon is scattered, a new movement distance is computed, and the photon is moved to its new position where the process of weight reduction, direction, distance computation, and movement is repeated. Algorithms for computing scattering angles, direction and position are described by Welch and van Gemert (1995) and Keijzer et al., (1989). The process is continued until the weight of the photon becomes small (about 0.001 of the original weight) or the photon leaves the tissue, then a new photon is introduced. A complete description of the algorithm with sample calculations may be found from Welch and van Gemert (1995) and Keijzer et al. (1989).

Photon propagation in multilayers is achieved by keeping track of the position of the weighted photon. If the movement interval Δs crosses a boundary, a new $\Delta s'$ is calculated that takes into consideration the optical properties of both layers (Welch and van Gemert, 1995).